Earth and Planetary Science Letters 506 (2019) 371–380

Contents lists available at ScienceDirect

Earth and Planetary Science Letters

www.elsevier.com/locate/epsl

Can active sands generate dust particles by wind-induced processes?

Nitzan Swet [a,*], Tov Elperin [b], Jasper F. Kok [c], Raleigh L. Martin [c], Hezi Yizhaq [d], Itzhak Katra [a]

[a] Department of Geography and Environmental Development, Ben Gurion University of the Negev, Be'er-Sheva, Israel
[b] Department of Mechanical Engineering, The Pearlstone Center for Aeronautical Engineering Studies, Ben-Gurion University of the Negev, Be'er-Sheva, Israel
[c] Department of Atmospheric and Oceanic Sciences, University of California, Los Angeles, USA
[d] Department of Solar Energy and Environmental Physics, BIDR, Ben-Gurion University of the Negev, Israel

ARTICLE INFO

Article history:
Received 10 June 2018
Received in revised form 28 October 2018
Accepted 4 November 2018
Available online xxxx
Editor: J.P. Avouac

Keywords:
aeolian processes
dust sources
PM_{10}
wind tunnel
saltation

ABSTRACT

Mineral dust emission is a major process in determining the global dust cycle. At a global scale there is still uncertainty about the absolute and relative contribution of dust from different source areas and landforms. Dust sources are mainly considered as surfaces containing relatively high percentages of fine particles (e.g. Playas). Yet, active (dune) sands have been identified recently, by remote sensing studies, as dust sources in northern Africa, China, and elsewhere. Previous studies on dust emission from active sands suggested that dust can be generated by different aeolian mechanisms that are related to (i) re-emission of settled dust particles, (ii) clay coating removal, and (iii) abrasion of the sand grains. However, there is only limited information of the relative importance of the different mechanisms for producing this dust under natural aeolian (wind) conditions. This study integrates wind tunnel experiments and high resolution laboratory sand analyses to explore aeolian dust emission from active sands with conditions simulating the natural processes of saltation and explores the role of the different dust emission mechanisms. Sand samples from three sites with different characteristics of grain size, dust content, morphology, and mineralogy were used in the experiments. No dust emission was recorded for shear velocities below the saltation threshold. The initial content of dust-sized particles (>63 μm) in the sand sample was found to influence PM_{10} emission. PM_{10} concentrations were increased with the initial content of dust-sized particles in the sand. The experiments identify clay coatings removal as the dominant mechanism over time of dust emission in typical active sand dunes (<2% dust content) with an addition of re-emission of existing dust-sized particles (<63 μm). The results also suggest that aeolian abrasion play only a minor role in PM_{10} dust generation from active sands, producing mostly relatively course dust-sized particles (>40 μm). The dust emission observed in this study indicates that, in addition to the classic dust sources of non-sandy soils, sand bodies should also be taken into consideration in determining global dust emission.

1. Introduction

Aeolian (wind-driven) dust emission has a major impact on a variety of environmental and socioeconomic issues. Airborne dust particles can affect climate (Nenes et al., 2014; Kok et al., 2017), biogeochemical cycles (Jickells et al., 2005), and soil ecology (Okin et al., 2004; Field et al., 2010). Substantial loss of nutrients and clays by dust emission reduces the soil fertility, leading to soil loss and degradation (Katra et al., 2016a). Dust events significantly increase air pollution (Katra et al., 2014a; Krasnov et al., 2016) and thus can impact human health (Vodonos et al., 2015). Models estimate that the global dust emission rate is between ~500 $Tg\,yr^{-1}$ and ~4000 $Tg\,yr^{-1}$ (Evan et al., 2015; Huneeus et al., 2010; Kok et al., 2014a, 2017; Shao et al., 2011). Comparisons of model results against dust measurements still show large discrepancies (Evan et al., 2014; Huneeus et al., 2010; Kok et al., 2014b) due to a number of major gaps in our understanding of dust source dynamics and mechanisms of dust emission. It is commonly assumed that dust sources consist of soils rich in clay and silt sized particles (<63 μm in diameter). These fine particles are subjected to cohesive inter-particle forces and therefore rarely occur as loose particles in soil but as part of aggregates. Therefore, impacts by saltating particles (sandblasting) have been found to play a major role in dust emission from aggregated

* Corresponding author.
E-mail addresses: swet@post.bgu.ac.il (N. Swet), elperin@bgu.ac.il (T. Elperin), jfkok@ucla.edu (J.F. Kok), raleighmartin@gmail.com (R.L. Martin), hezi.yizhaq1@gmail.com (H. Yizhaq), katra@bgu.ac.il (I. Katra).

https://doi.org/10.1016/j.epsl.2018.11.013
0012-821X/

soils (Alfaro et al., 1997; Kok et al., 2012, 2014a; Shao et al., 1993; Shao, 2008; Swet and Katra, 2016).

Little attention has been paid to the contribution of active sand dunes as dust sources. Active sand refers to un-stabilized (loose) sand-sized particles that are available for wind transport. The possibility to generate dust, i.e., clay (<2 μm in diameter) and silt (between 2 and 63 μm in diameter) sized particles from active sands has been suggested over the years. Most studies dealing specifically with active sand have proposed aeolian abrasion of the grains as the mechanism for dust generation (Bhattachan et al., 2012; Bullard et al., 2004; Crouvi et al., 2012; Sweeney et al., 2016; Wright et al., 1998). However, none of these studies have proven the existence of this mechanism under natural aeolian conditions. Dust that is apparently generated by active sands may also be produced through other mechanisms: re-emission of dust previously trapped in dunes from exogenous sources (Muhs et al., 2008), and/or by the detachment of clay-rich coatings present on the surfaces of sand grains (Bullard and White, 2005; Bullard et al., 2007). Studies have shown that many of the sand bodies worldwide contain sand with clay and iron oxide coatings (Walden and White, 1997). The removal of these coatings during the saltation transport is often considered as a form of aeolian abrasion (Bullard et al., 2007). However, here we define aeolian abrasion as the reduction in the physical size and angularity of parent sands due to the impact of saltators at the sand bed or by particle collisions in the air (Bagnold, 1937; Jerolmack and Brzinski, 2010; Jerolmack et al., 2011; Kuenen, 1960).

A recent remote sensing study identified that over 40% of dust storms in Northern Africa originate from areas covered by sand dunes (Crouvi et al., 2012). The occurrence of fine particle production from sand has also been deduced from field (Crouvi et al., 2008, 2012; Jerolmack and Brzinski, 2010; Jerolmack et al., 2011; Sweeney et al., 2016) and experimental (Bullard et al., 2004, 2007; Bullard and White, 2005; Kuenen, 1960; Smalley and Vita-Finzi, 1968; Whalley et al., 1982; Wright, 2001) studies. Field studies proposing aeolian abrasion as the primary generator of dust particles are based on identification of downwind fining of aeolian sediment. However, the observed spatial fining trends may also result from sorting or fractionation caused by differences in transportability of different grain sizes (Roskin et al., 2014). In addition, the few existing studies on dust generation from active sand were performed under conditions that do not directly reproduce the natural processes of saltation. Thus, our understanding of aeolian dust emission from sands remains limited.

Sand dunes cover around 20% of arid areas worldwide, and about half of them are considered as active sand dunes (Ashkenazy et al., 2012; Pye and Tsoar, 2009). Sand dunes are also a dominant formation covering wide areas of Mars, Venus and Titan (Claudin and Andreotti, 2006; Charnay et al., 2015; Runyon et al., 2017). Typical active sand dunes are characterized by more than 98% of sand-sized grains (63–2000 μm) with a size distribution mode of 200–300 μm (Ahlbrandt, 1979). In addition to sand dunes, there are other forms of active sand with different particle composition. Sandy soils contain relatively high percentages of clay-silt particles (up to ∼10%). Many of these arid soils are located in close proximity to dust sources and are subjected to aeolian deposition of airborne dust. Another sand form is mega-ripple fields composed of fine sand and very coarse sand with a mode of up to 2000 μm (Yizhaq and Katra, 2015). It can be hypothesized that different active sand compositions will respond differently to aeolian processes and produce different rates and types of dust emission over time.

Understanding the role of active sand as a dust source can provide a more accurate estimation of quantities and particle characteristics of global dust loading to the atmosphere, thereby reducing uncertainties in chemical transport and global climate models. It can also contribute to our understanding of sand transport and landscape development on Earth, Mars, and other planetary bodies. The aim of this study is to quantify dust emission from active sands under different conditions simulating the natural processes of saltation. The study integrates targeted laboratory experiments and sand analyses to fill this apparent research gap.

2. Materials and methods

2.1. Sand samples

Three samples of active sand were utilized to represent different sand particle compositions. Sand was collected from two dunefields in the northwestern Negev (N_1 and N_2), Israel, and from Oceano Dunes, California (C_1). In both sites there is an ongoing in-situ study of dust emission for data comparison. In addition, these sites have been extensively studied in the past and there is prior information on sand transport and source.

The Negev dunefield is located in the eastern part of the Sinai–Negev erg (Fig. A1). Currently some dunes are partially stabilized by biological crusts, but their crests are still active (Tsoar et al., 2008; Zaady et al., 2014). The Negev dune sand has a typical size of sand for active dunes (mode at ∼250 μm; Roskin et al., 2014). The N_1 sample was taken from an active linear sand dune, and contains less than 2% (by volume) of clay and silt-sized particles. N_2 was sampled in sand at the northernmost edge of the Negev dunefield. The sand of N_2 is composed of active sand with relatively high percentages of silt and clay sized particles (<63 μm) of up to 10%. The higher amount of dust in N_2 compared with N_1 is due to the proximity of N_2 to the Negev loess plane. Nevertheless, this region is associated with particle-size fractionation of aeolian sand transport along the Sinai–Negev erg (Roskin et al., 2014).

The Oceano dunefield on the Central Coast of California (Fig. A1) was formed by strong onshore sea breezes transporting sand derived from fluvial deposits (Cooper, 1967), and thus contains a mixture of quartz, feldspar, and other minerals (Huang et al., 2018; Bedrossian and Schlosser, 2007). The sample from C_1 is composed of relatively coarse sand particles (mode >400 μm) with low amount (<1%) of dust sized particles (Huang et al., 2018; Martin et al., 2018). Sand samples from each site were taken from the upper 2-cm layer of the dunes for wind tunnel experiments and laboratory analyses.

2.2. Aeolian experiments

Laboratory wind tunnel experiments were performed to quantify dust emission from the sand samples. The experiments were conducted under various wind velocities, above and below the saltation threshold, to examine two components of dust emission: re-emission of loose dust particles in the sand samples by direct aerodynamic lifting (no saltation), and dust emission caused by saltation impacts onto the sand surface. For each wind velocity and sand sample, the wind profile was measured at different heights (cm) above the tunnel bed: 2, 3.5, 5, 7.5, 10, 15, 20, 25, 30, 35, 40, and 45 (Fig. A2). These wind profiles were used for determining shear velocities (u_*, $m\,s^{-1}$) following the logarithmic *law of the wall*.

The aeolian experiments were performed using the boundary-layer wind tunnel of Ben-Gurion University (BGU) described in Katra et al. (2014b). The BGU wind-tunnel is an open circuit tunnel consisting of three parts: an entrance cone, a test section, and a diffuser (Fig. A2). Air is sucked in through the bell-shaped entrance by a fan located at the end of the diffuser. The cross sectional area of the tunnel is ∼0.7 ×0.7 m and the working length is 7 m for measurements in the test section. The boundary layer in the wind tunnel is ∼22 cm above the tunnel bed (Fig. A2). For each experimental run at a specific shear velocity, the saltation flux remains constant (±10%) and does not fade or intensify

over time (Katra et al., 2014b; Schmerler et al., 2016). Instruments installed in the wind tunnel enable the determination of the following parameters (Fig. A2B): (i) wind velocity in vertical and horizontal cross sections by micro-vane probes (www.kimo.com) for calculation of shear velocity (u_*); (ii) collection of saltating sand grains by an array of traps oriented along the wind direction for calculating average saltation mass flux ($kg\,m^{-1}\,s^{-1}$) over time. The traps were placed at heights of 2.5, 4.5, 6.5, 8.5 and 10.5 cm above ground, and each trap had a cross-sections of 2 × 1 cm; (iii) dust concentrations ($\mu g\,m^{-3}$) of particles that are less than 10 μm in aerodynamic diameter (PM_{10}) recorded by a light-scattering device, DustTrak DRX 8534 (www.tsi.com), in the range of 0.001–150 $mg\,m^{-3}$ (±0.1% of reading) at 1-s intervals, placed at 25 cm above the tunnel bed; (iv) collection of suspended dust by active (isokinetic filter) gravimetric samplers that include a pump to maintain a constant flow and an inertial Anderson impactor (Andersen Instruments Inc., USA) for dust characteristic analyses.

In each experiment, the sand was placed in a ∼3-cm thick layer on the full length of the wind tunnel bed. The first test was conducted under a free stream wind speed of 4 $m\,s^{-1}$, corresponding to a shear velocity of 0.28 $m\,s^{-1}$, below the saltation threshold for each sample. The test was run for a relatively short time of 900 s. The second test was run under higher wind shear velocities and above the saltation threshold of the different samples, at $u_* = 0.30$–0.36 $m\,s^{-1}$ (∼5 $m\,s^{-1}$ to ∼8.5 $m\,s^{-1}$, measured at 25 cm above the tunnel bed). In this case, dust emission can be a result of sand abrasion and/or removal of coatings, but also by aerodynamic lifting of loose particles that are held between the coarser sand grains and may be released upon their movement or impacts during the saltation transport. The time duration of each experiment (shear velocity) was up to 9000 s (150 min), which is much longer than a single wind shear velocity would typically be sustained in the field. Wind events can last for hours, but the cumulative time of specific shear velocity at a specific direction will be significantly shorter.

Before each experiment, the PM_{10} background levels were measured inside the tunnel to account for noise in the measured PM_{10} signal. The measured background levels (∼0.30 $\mu g\,m^{-3}$) were subtracted from the data recorded during the experiment. In order to optimize the measurement procedure, the sand was manually recycled in the tunnel during these long tests to allow a sufficient sand supply and ensure a saturated airstream and steady-state saltation. Each test was repeated 3 times to determine the mean values of saltation and dust emission. The recorded PM_{10} concentrations were converted into mass flux (F_{PM}) emitted from the soil surface ($kg\,m^{-2}\,s^{-1}$) based on the wind tunnel dimensions and area of the sand bed:

$$F_{PM} = C_{PM} V_t / (A_p t) \quad (1)$$

where C_{PM} is the recorded PM concentrations ($\mu g\,m^3$), V_t is the volume air in the wind tunnel (3.43 m^3), A_p is the area of the experimental plot (4.9 m^2), and t is time (in seconds), see Katra et al., 2016b. The PM_{10} ($kg\,m^{-2}\,s^{-1}$) was used to calculate the sand-blasting efficiency a (m^{-1}):

$$a = F_{PM} / Q \quad (2)$$

where Q ($kg\,m^{-1}\,s^{-1}$) is the total horizontal sand flux integrated over all sand grain sizes (see Kok et al., 2014a).

All of the above procedures were performed also on dust-free 'clean' sand to separate between the mechanisms of dust emission. The raw sand (bulk samples) underwent a series of gentle rinsing and washing to remove the loose dust-sized particles. Following the results obtained for the bulk samples (see section 3; Fig. 3), in which the dust emission of C_1 sample stopped after a period of time (reduced to the background values), and following a preliminary experiment on 'clean' sand from C_1 sample, in which no dust emissions were detected, the wind tunnel experiments on 'clean' sand were conducted only for N_1 and N_2 samples.

2.3. Particle analyses

Physical and chemical properties of the sand (from the tunnel bed before the aeolian experiments and from the sand traps during the experiments) and of the dust (collected during the experiments) were analyzed in the laboratory.

The Particle Size Distribution (PSD) was analyzed using an ANALYSETTE 22 MicroTec Plus (Fritsch) laser diffractometer, which measures particles in the size range of 0.08–2000 μm. PSD data were calculated using the Fraunhofer diffraction model with a size resolution of 1 μm using MasControl software. The software was employed to determine the mean diameters, median diameters, modes of multi-modal distributions, sorting values, and size fraction weights. Mineralogical composition was analyzed using the X-ray power diffraction (XRPD) method (Philips 1050/70 power diffractometer). A Panalytical Empyrean Powder Diffractometer equipped with position sensitive detector X'Celerator was used. Data were collected in the $\theta/2\theta$ geometry using Cu K_α radiation ($\lambda = 1.54178$ Å) at 40 kV and 30 mA. Scans were run during ∼15 min in a 2θ range of 4–60° with step equal to ∼0.033°. Elemental composition analyses were performed by the X-Ray Fluorescence (XRF) method using an XRF spectrometer PANalytical Co., model Axios (wavelength dispersive-WDXRF, 1 kW). The Omnian software was used for the quantitative analysis. Morphological and chemical characteristics of the particles were examined using a Scanning Electron Microscope (SEM) (Quanta 200, FEI). The high magnification (6 × to >1,000,000 ×) enabled the analysis of the smallest dust particles (<2 μm). Chemical analysis in this device was performed using the Energy Dispersive X-ray Spectroscopy (EDS). Sand-grain roundness was assessed for each SEM image using the grain roundness chart of Powers (1953).

3. Results

The PSDs of the three bulk samples used in the aeolian experiments are presented in Fig. 1. All the samples are characterized by a distribution with a single mode in the range of sand-sized particles. However, there are significant differences ($P \leq 0.05$) in the size mode and in the initial dust content between the samples. N_1 contains a relatively high percentage (58.7%) of medium-sized sand (250–500 μm), whereas N_2 is characterized by a relatively large amount (64.4%) of fine sand (63–250 μm) compared to the N_1 dune (23.5%). C_1 has a much coarser composition with 44.7% of sand larger than 500 μm. All the samples contain dust-sized particles (<63 μm) that can be found between or attached to the sand grains. N_2 dune can be considered as a "dusty" sand sample with 8.00% content of dust-sized particles as opposed to only 1.81% in N_1 and 0.95% in C_1 (Fig. 1). In all the samples, over 60% of the dust sized fraction is fine particles (<20 μm), which are subject to long-term suspension (Kok et al., 2017). The PM_{10} part, out of the dust content, is 64% in N_2 and ∼40% in N_1 and C_1 samples.

Mineralogical analyses (XRPD) of the samples show that N_1 and N_2 consist of over 90% quartz sand grains, while the C_1 sample is a mixture of quartz (45%) and feldspar (K-silicate 30% and Na-silicate 22%) grains. From the SEM images it seems that N_1 and N_2 sand grains are characterized as sub-rounded grains with a relatively smooth surface (Fig. 2A, B). C_1 is composed of mostly sub-angular and angular sand grains (Fig. 2C). The feldspar sand grains look more angular and their surfaces are more abraded compared with the surfaces of the quartz sand grains (Fig. 2C). Clay and iron-rich coatings are found on top of the sand grains in all of the tested

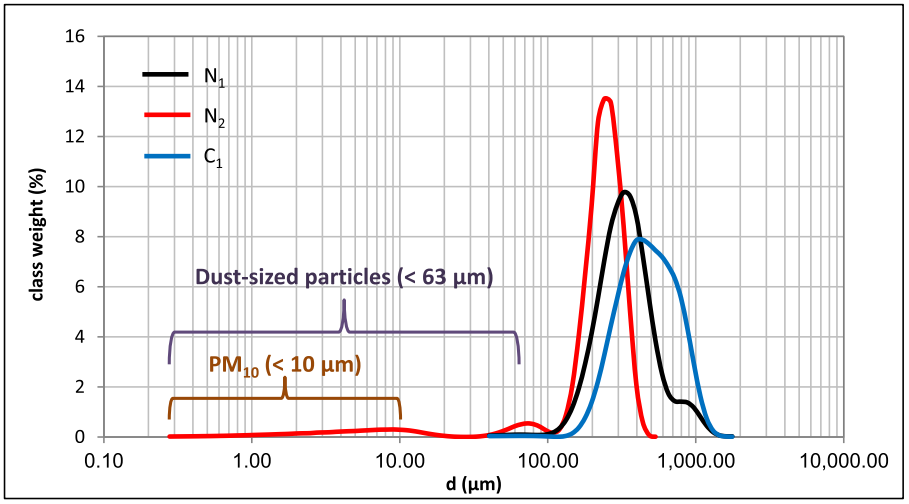

	N_1	N_2	C_1
Statistical parameters (µm)			
Mean	389.02	242.07	538.28
Mode	342.38	254.01	461.48
D10	200.15	125.77	270.61
D50	346.10	249.33	490.95
D90	620.44	350.27	879.67
Fraction weight (%)			
Clay (< 2 µm)	0.22	1.41	0.16
Fine-silt (2-20 µm)	0.92	4.80	0.41
Coarse-silt (20-63 µm)	0.67	1.79	0.38
Dust-sized (< 63 µm)	1.81	8.00	0.95
Fine sand (63-250 µm)	23.45	64.44	7.93
Medium sand (250-500 µm)	58.69	21.51	46.42
Coarse-sand (> 500 µm)	16.05	0.00	44.69
Sand (63-2000 µm)	98.19	91.95	99.04
Environmental PM (%)			
PM_1 (< 1 µm)	0.12	0.64	0.09
$PM_{2.5}$ (< 2.5 µm)	0.26	1.71	0.19
PM_{10} (< 10 µm)	0.75	3.29	0.41

Fig. 1. Average particle size distribution (PSD) of sand from N_1, N_2 and C_1 sites obtained by the laser diffraction technique. On the right side are statistical parameters of the distributions. The sample PSDs are significantly different with $P < 0.05$.

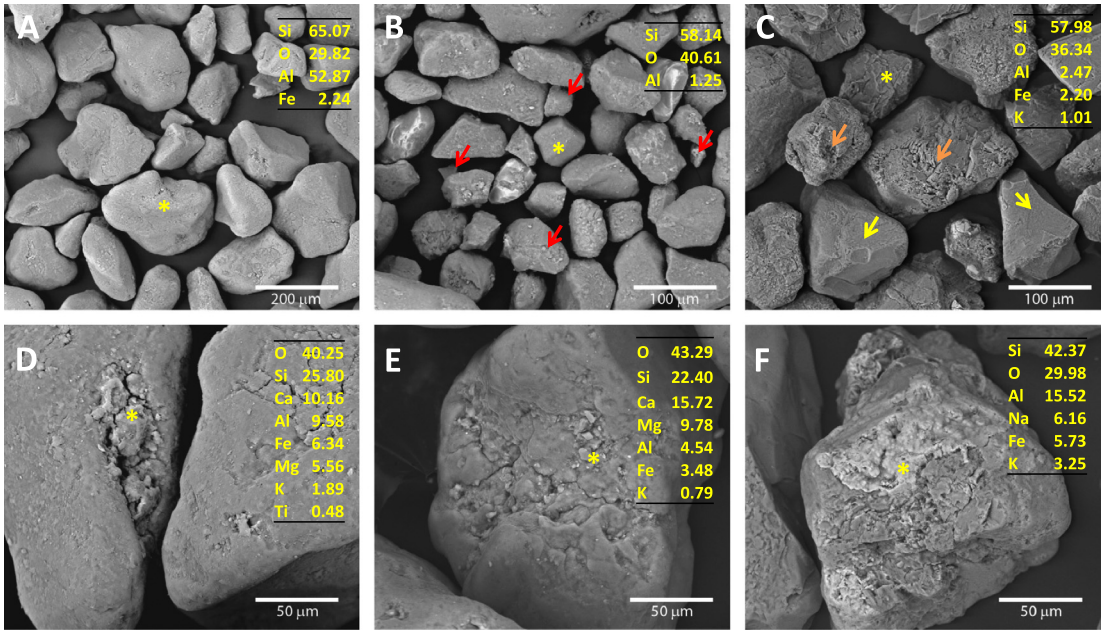

Fig. 2. Scanning electron microscope (SEM) images of sand particles collected from N_1 (A), N_2 (B) and C_1 (C) sand samples. The red arrows in A point to dust-sized particles (<63 µm) found between the sand grains. In C the yellow arrows point to quartz grains, while the orange arrows point to feldspar sand grains. D–F are close-up images of the coatings attached to sand particles from N_1, N_2 and C_1, respectively. In the yellow box is a chemical composition analysis (%) using SEM-EDS. The location of the EDS analysis is marked by an asterisk. (For interpretation of the colors in the figure(s), the reader is referred to the web version of this article.)

samples (Fig. 2D, E, F). Clay minerals were found also as part of the loose dust-sized particles (<63 µm) within the sand samples (Fig. 2A).

Subjecting the bulk N_1, N_2, and C_1 samples to a range of wind velocities in the boundary layer wind tunnel (Fig. 3) revealed a distinct pattern in the measured atmospheric PM_{10} concentrations ($\mu g\,m^{-3}$), depending on initial dust content in the sand sample, shear velocity, and saltation flux (Fig. 1; Table 1). At low wind shear velocities below the saltation threshold of all samples ($<0.29\ m\,s^{-1}$), no PM_{10} emissions were recorded (Figs. 3A, C, E). The threshold shear velocities were measured by a careful and gradual increase of the wind velocity in the tunnel to the moment of which the sand grains entered saltation transport. The recorded thresholds were $0.29\ m\,s^{-1}$ (N_2), $0.30\ m\,s^{-1}$ (N_1), and $0.33\ m\,s^{-1}$ (C_1). Notably, the wind-tunnel observed threshold at C_1 is similar to the $0.32\ m\,s^{-1}$ fluid threshold shear velocity calculated independently from field measurements by Martin and Kok (2018). At a wind shear velocity of $0.30\ m\,s^{-1}$, PM_{10} emission was recorded only in the N_2 sand (Fig. 3C) as a response to the initiation of saltation transport (Table 1). In the N_1 and C_1 samples, this wind was not sufficient for dust emission (Fig. 3A, E). In the N_1 sample, only a small amount of sand grains were ejected into saltation, while no sand transport was observed in the C_1 sample (Table 1). Increasing the wind shear above the saltation threshold ($\geq 0.33\ m\,s^{-1}$) resulted in dust emission and enhanced PM_{10} concentrations for all sand samples. For each constant shear velocity experimental run, the dust emission over time was characterized by a distinct pattern of an initial sharp rise in PM_{10} concentrations, followed by a gradual decline until stabilizing at low values (Fig. 3B, D, F). However, clear differences in PM_{10} concentrations can be detected between the sand samples (Fig. 3B, D, F). The average PM_{10} concentration produced by the N_2 sample was ~8 times

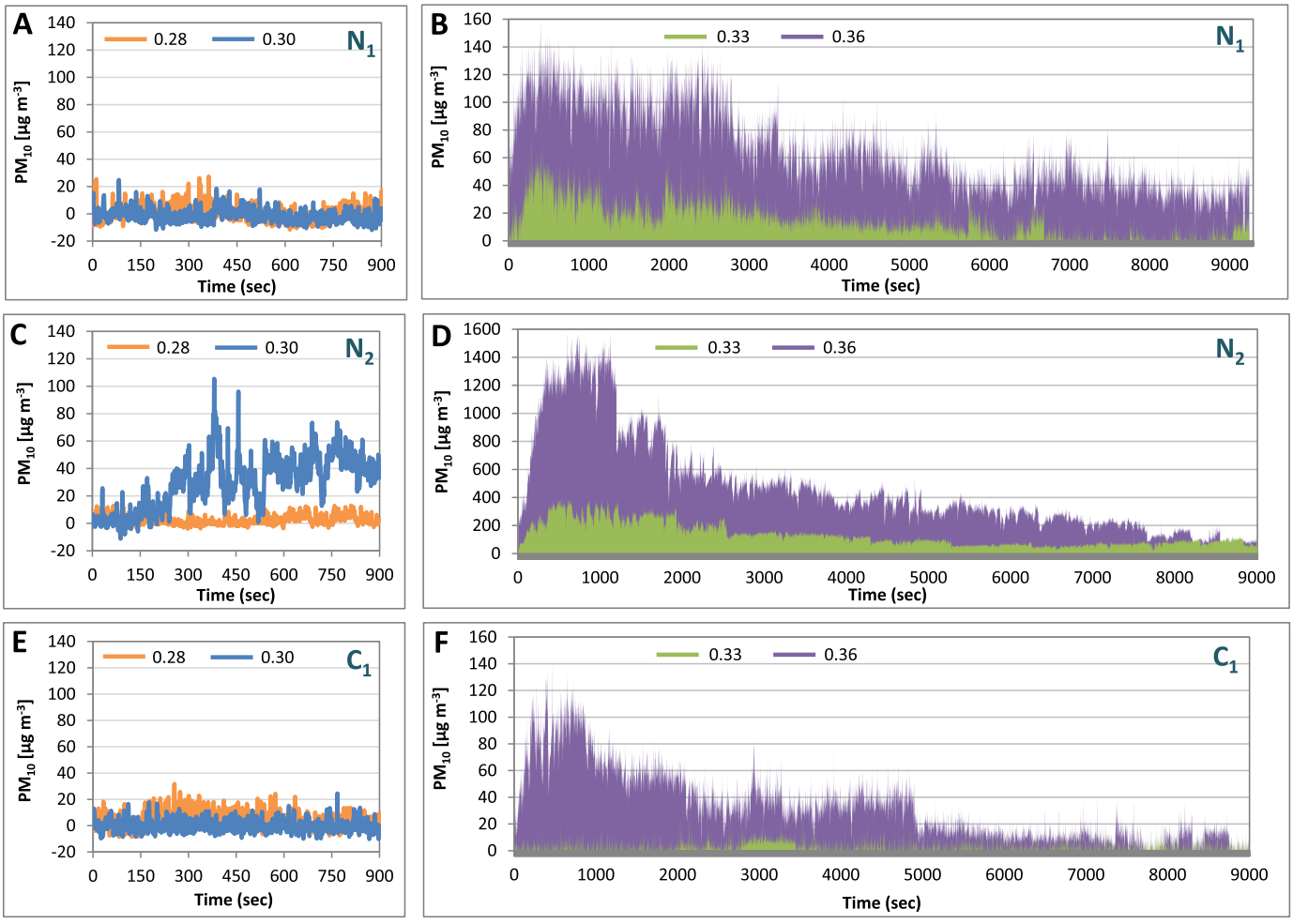

Fig. 3. PM_{10} concentrations [$\mu g\,m^{-3}$] following dust emission in the wind tunnel under various shear velocities in N_1 (top), N_2 (middle), and C_1 (bottom). (A), (C) and (E) show results of the experiments at the lower shear velocities (u_* of 0.28 and 0.30 $m\,s^{-1}$), for convenient display of the results; (B), (D) and (F) show dust emission over time (9000 s) at the higher shear velocities of 0.33 $m\,s^{-1}$ and 0.36 $m\,s^{-1}$. Note the different Y axis scales. The PM_{10} concentrations are after the background values were subtracted. The net concentrations in A, C, and E are sometimes negative because they are statistically indistinguishable from the background.

Table 1
Saltation flux by mass ($kg\,m^{-1}\,s^{-1}$) of the bulk and the 'clean' sand; average atmospheric PM_{10} concentration ($\mu g\,m^{-3}$) due to emitted PM_{10} flux ($kg\,m^{-2}\,s^{-1}$) from the bed (average PM_{10} flux in brackets); and sandblasting efficiency (m^{-1}) during the aeolian experiments under the different shear velocities (0.28–0.36 $m\,s^{-1}$). The background values were subtracted from the PM_{10} concentrations and fluxes. Note the different duration of the aeolian experiments, 900 s for 0.28–0.30 $m\,s^{-1}$ and 9000 s for 0.33–0.36 $m\,s^{-1}$. In all the experiments, the saltation rate remained approximately constant (±10%) while the PM_{10} concentration and flux reduced over time.

	0.28	0.30	0.33	0.36
N_1 saltation	0.00	1.46×10^{-4}	1.27×10^{-3}	2.13×10^{-3}
N_2 saltation	0.00	1.22×10^{-3}	1.19×10^{-3}	2.29×10^{-3}
C_1 saltation	0.00	0.00	8.53×10^{-4}	5.68×10^{-3}
N_1 PM_{10}	0.00	0.01 (1.66×10^{-10})	13.64 (9.17×10^{-9})	66.08 (4.52×10^{-8})
N_2 PM_{10}	0.00	28.65 (5.66×10^{-9})	248.34 (8.92×10^{-8})	1065.86 (3.24×10^{-7})
C_1 PM_{10}	0.00	0.00	4.00 (6.67×10^{-10})	23.36 (2.03×10^{-8})
N_1 efficiency	N/A	1.73×10^{-7}	4.64×10^{-6}	1.37×10^{-5}
N_2 efficiency	N/A	3.88×10^{-5}	7.03×10^{-5}	1.52×10^{-4}
C_1 efficiency	N/A	N/A	7.81×10^{-7}	3.58×10^{-6}

higher than by N_1, although both sand samples produced very similar saltation fluxes (Table 1). The saltation flux (Table 1) of the courser saltating particles of C_1 (418 µm; Fig. 4) was found to be greater than in N_1 and N_2 samples under shear velocity of 0.36 $m\,s^{-1}$, although the amount of particles entering transport is expected to be lower than in N_1 and N_2 samples. However, the calculated sandblasting efficiency (m^{-1}), which is the ratio of the dust emission flux ($kg\,m^{-2}\,s^{-1}$) to the sand saltation flux ($kg\,m^{-1}\,s^{-1}$), is substantially smaller for C_1 than for the samples from the other sites under all shear velocities. In all samples there was an increase in sandblasting efficiency with shear velocity (Table 1). The highest efficiency obtained was for the N_2 sample, although associated saltation fluxes were similar to those from the N_1 sample. The efficiency recorded for the C_1 sample is considered as relatively low but similar to those found in a field experiment in Oceano dunes (10^{-6} m^{-1}; Huang et al., 2018). The sandblasting efficiency

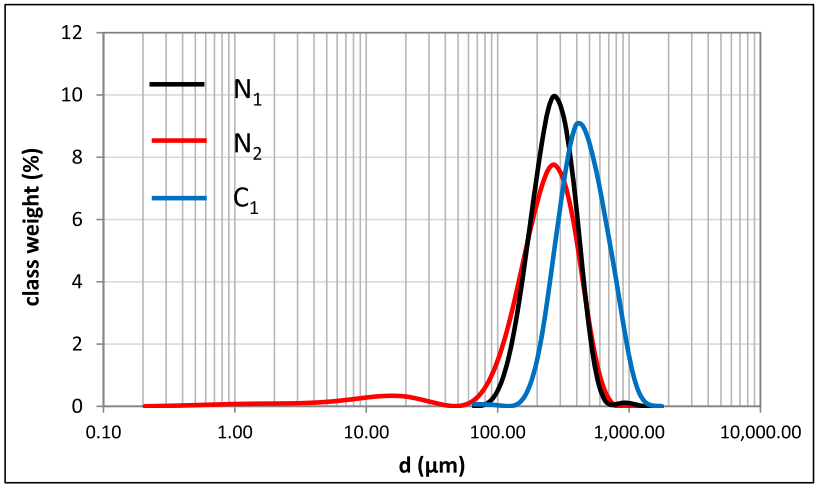

	N_1	N_2	C_1
Statistical parameters (µm)			
Mean	295.46	262.82	507.40
Mode	280.59	280.59	417.77
D10	165.02	101.48	271.97
D50	278.00	250.30	462.55
D90	443.20	448.13	810.09
Fraction weight (%)			
dust (< 63 µm)	1.45	7.45	0.39
Fine sand (63-250 µm)	43.72	46.32	8.42
saltators (63-500 µm)	95.16	88.31	61.07
Coarse-sand (> 500 µm)	3.40	4.24	38.53

Fig. 4. Average particle size distribution (PSD) of the sand collected from the **saltation traps** after the wind tunnel experiments ($u^* = 0.33\ \mathrm{m\,s^{-1}}$) for N_1, N_2 and C_1 dune samples. On the right are statistical parameters of the distributions ($P \leq 0.05$).

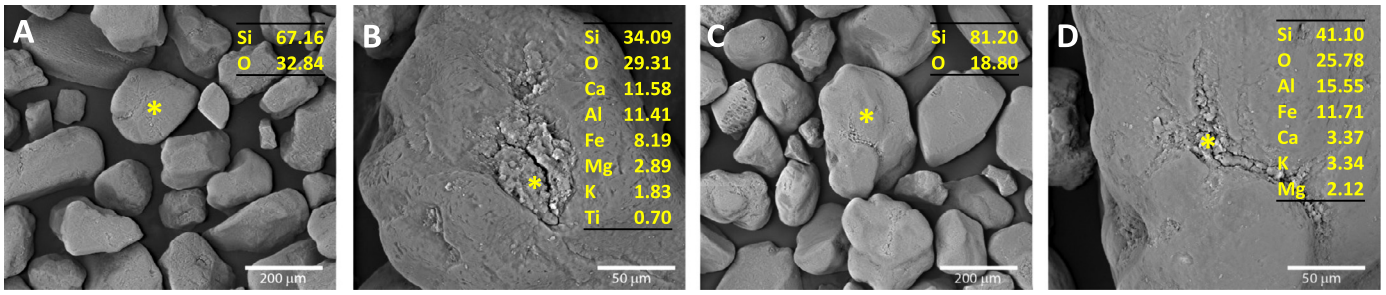

Fig. 5. Scanning electron microscope (SEM) images of the clean sand N_1 (A) and N_2 (C). B and D are close-up images of the coatings attached to a sand particle. In the yellow box is a chemical composition analysis (%) using SEM-EDS. The location of the EDS analysis is marked by the asterisk.

reduces in all sand samples as the PM_{10} emission decreases over time, while the saltation flux remains constant. The efficiency results obtained for all of the sand samples (10^{-7} to 10^{-4} $\mathrm{m^{-1}}$) were found as smaller than typical non-sandy soils (10^{-4} to 10^{-2} $\mathrm{m^{-1}}$) (Kok et al., 2012).

Following the results of the bulk sand samples (Fig. 3), only N_1 and N_2 samples were washed of loose dust particles to examine the emission mechanisms. The cleaning of the sand samples did not have any mineralogical, chemical, or physical effect on the sand grains or on the coatings on the grain surfaces (Fig. 5). The cleaning of the sand only reduced the amount of dust-sized particles in the sand to a minimum of no more than 0.6% in both N_1 and N_2 samples (Table A1). The PM_{10} concentrations produced from the 'clean' sand were lower than those from the bulk samples (Fig. 6), while the saltation fluxes did not change (2.89×10^{-3} $\mathrm{kg\,m^{-1}\,s^{-1}}$ for 'clean' N_1 and 2.98×10^{-3} $\mathrm{kg\,m^{-1}\,s^{-1}}$ for 'clean' N_2). The resulted dust emission from N_1 and N_2 'clean' sand samples show similar PM_{10} concentrations (red line, Fig. 6) with 56.5 $\mu\mathrm{g\,m^{-3}}$ and 60.5 $\mu\mathrm{g\,m^{-3}}$, respectively.

The dust emitted during the aeolian experiments was collected for laboratory analysis (Fig. 7). The SEM images indicate that the emitted dust from the N_1 and N_2 bulk samples are composed mostly of clay minerals (Fig. 7A, B). The chemical and mineralogical composition of the emitted dust of the bulk samples was similar to that of the loose dust-sized particles found between sand grains and to the coatings on top of the grain surfaces (Fig. 2). Only a few isolated quartz fragments were found among the dust particles. In the C_1 sample, the emitted dust consists of a mixture of clays, feldspar, and quartz particles, in comparable quantities (Fig. 7C). The quartz fragments were relatively coarser (30–40 µm) than the feldspar and the clay particles (<20 µm). The analysis of the emitted dust from the 'clean' sand samples (N_1 and N_2) show similar composition to those of the bulk samples, with mostly clay minerals and only some single coarser quartz fragments (>40 µm) (Fig. 7D, E).

4. Discussion

By subjecting three distinctive natural sand samples to a range of wind strengths in a laboratory wind tunnel, we were able to simulate the process of dust emission from active sands during aeolian saltation. Throughout the experiments, it was found that dust emission from the sand samples was directly associated with the occurrence of saltation transport, where PM_{10} emission occurs only in the presence of saltation (Fig. 3; Table 1). As such, direct aerodynamic entrainment of dust was not detectable. Dust emission from active sand in our experiments thus requires that wind strength exceeds the threshold shear velocity, which in turn depends on the surface PSD (Bagnold, 1937; Kok et al., 2012; Schmerler et al., 2016). In the N_2 sample, the PSD (mode of 251 µm) is finer than for the N_1 and C_1 samples (modes at 342 µm and 461 µm, respectively), and therefore its threshold shear velocity is lower ($0.29\ \mathrm{m\,s^{-1}}$).

For a specific shear velocity and saltation flux, the dust emission flux appears to be primarily controlled by the dust-sized particle content of the sand surface. The results show that when the wind shear was strong enough ($\geq 0.33\ \mathrm{m\,s^{-1}}$) the saltation flux of N_1 and N_2 samples was similar (Table 1). However, the recorded PM_{10} and therefore the calculated sandblasting efficiency were much higher for N_2 than for N_1 (Table 1). The reason for these differences can be explained by the higher initial content of dust in the N_2 sand sample. N_2 contains relatively high amounts of dust-

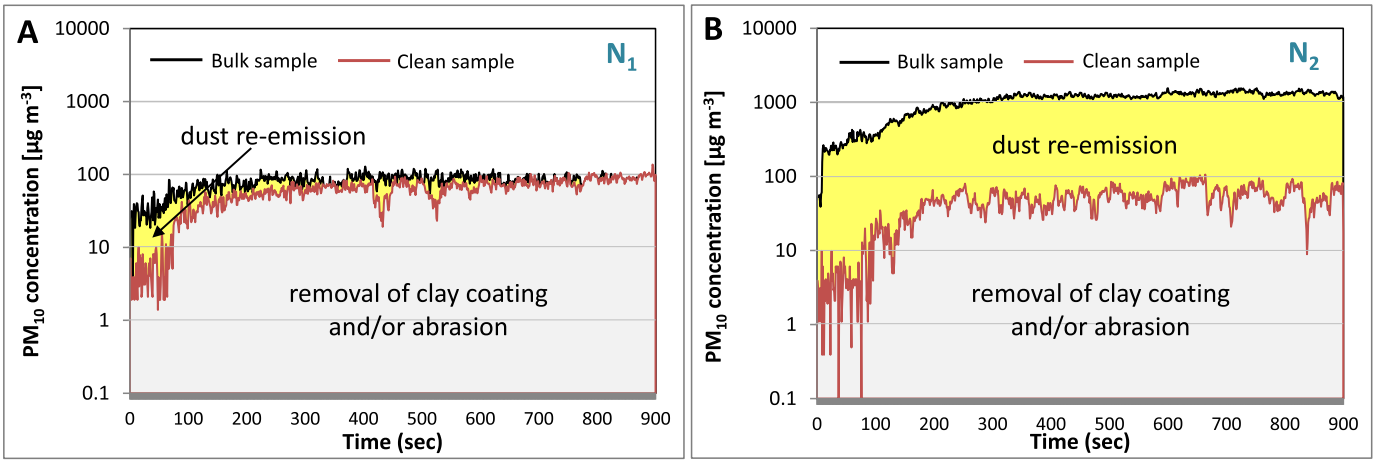

Fig. 6. PM_{10} concentration [$\mu g\,m^{-3}$] before (black) and after (red) loose dust removal by washing of the N_1 (A) and N_2 (B) samples under shear velocity (u_*) of 0.36 $m\,s^{-1}$. The background levels were subtracted from all measured PM_{10} concentration levels.

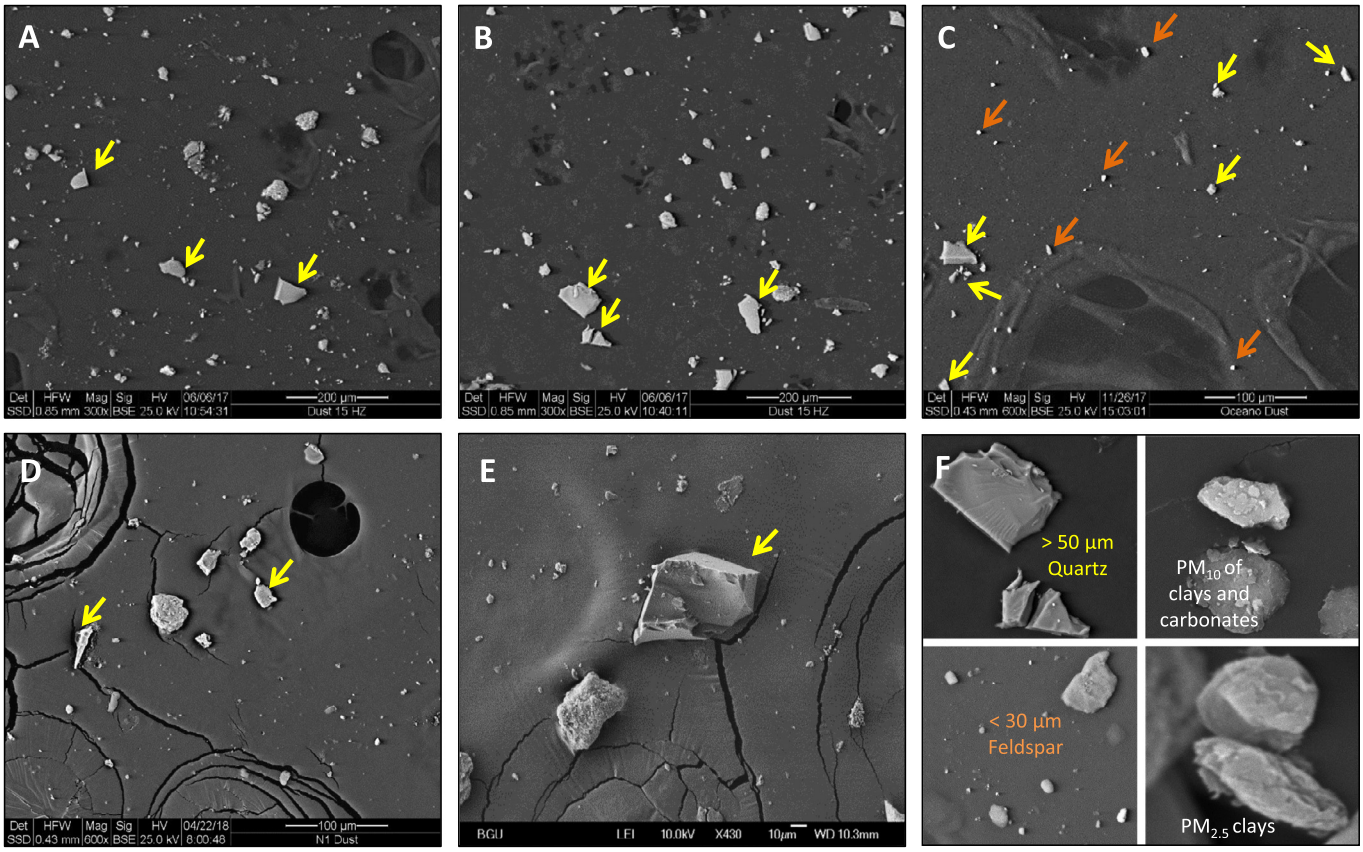

Fig. 7. Scanning electron microscope (SEM) images of the emitted dust collected during the aeolian experiments for shear velocity of 0.33 $m\,s^{-1}$ from N_1 (A), N_2 (B) and C_1 (C) samples. D and E are images of the emitted dust from the 'clean' sand of N_1 and N_2, respectively. The yellow arrows point to quartz fragments, while the orange arrows in C_1 point to feldspar dust size particles (<63 µm). All the remaining particles are composed of clay minerals with some carbonates and metallic materials. F is a close-up of different types of dust particles in the samples.

sized particles, especially PM_{10} particles (Fig. 1). It is hypothesized that the dust flux emitted per unit horizontal saltation flux increases sharply with the content of fine particles (Kok et al., 2014a; Marticorena and Bergametti, 1995). In the C_1 sample, for which the highest saltation fluxes were recorded, the PM_{10} concentration (and thus also sandblasting efficiency) was much lower. C_1 is composed of coarser sand with a mode of 417 µm (Fig. 1), and therefore the sand grains will enter into saltation transport only at higher wind velocities (Table 1), and thus dust emission will also be confined to higher wind velocities (Fig. 3), although the number of saltating particles for the C_1 sample can be much smaller than in N_1 and N_2 samples for a specific wind shear velocity. Therefore, the relatively low sandblasting efficiency of C_1, which is consistent with field measurements at the collection site (Huang et al., 2018), is likely related to the low initial PM_{10} content (0.41%).

The PM_{10} emission patterns observed in the wind tunnel experiments (Fig. 3) provide evidence for the relative importance of three possible dust emission mechanisms for sandy surfaces: (i) re-emission of previously settled dust particles in the sand (Muhs et al., 2008), (ii) clay coating removal from sand grains

(Bullard and White, 2005), and (iii) abrasion of the sand grains (Bhattachan et al., 2012; Bullard et al., 2007; Sweeney et al., 2016; Wright et al., 1998). The sharp increase in dust concentrations obtained at the beginning of saltation (Fig. 3B, D, F) can be generated from one or all of mechanisms listed above. However, the subsequent gradual decrease in the PM_{10} concentrations may indicate gradual exhaustion of the limited supply of loose dust particles for direct re-emission as the saltation flux remains the same over time (Zhang et al., 2016). From the results it seems that N_1 and N_2 samples have comparable sand characteristics of mineralogy, grain roundness, and saltator PSD, in addition to the similar saltation fluxes (Fig. 2; Fig. 4; Table 1); thus, no difference is expected in the mechanism generating the dust emission. Therefore the differences observed in the sandblasting efficiency and thus in the PM_{10} emission (Table 1) can thus be related to the higher initial content of loose dust-sized particles in N_2 (Fig. 1).

Comparing the PM_{10} emission patterns of the bulk samples to those of the 'clean' sand samples can provide further evidence for the relative importance of the different dust emission mechanisms (Fig. 6). Both 'clean' sand samples of N_1 and N_2 emitted very similar and relatively low amounts of PM_{10} over time ($u_* = 0.36\ m\,s^{-1}$), while the bulk samples showed significant differences in PM_{10} concentration in the beginning of each experiment (Fig. 6). After a period of time when the loose dust is emitted, the dust emission from the bulk samples reaches the minimum value of the 'clean' sand emission of ~0.06–0.1 $\mu g\,m^{-3}$ (N_1 after ~300 s; N_2 after ~7000 s, Fig. 3). The differences in PM_{10} concentrations found between the bulk samples (Fig. 3) can be related to the initial amount of loose dust-sized particles in the sand (Fig. 1). Therefore it can be assumed that in typical dune sands like the N_1 sample, which contains <2% of dust-sized particles, the re-emission of loose dust is relatively minor (Fig. 6A) and the continuous PM_{10} emission over time (Fig. 3B, D) is controlled by clay coating removal and/or abrasion.

The analysis of the emitted dust particles collected during the aeolian experiments provides further evidence for the relative contributions of the different dust emission mechanisms. The dust emitted from the N_1 and N_2 bulk samples consisted mostly of very fine particles of clay minerals (Fig. 7A, B), indicating similar primary dust sources from loose dust particles contained in the pore spaces among sand bed grains and from the coatings on these sand grains (Fig. 2). The fact that the dust emitted from the 'clean' sand of both N_1 and N_2 samples had barely any PM_{10} quartz particles (Fig. 7D, E), and that the clay dust particles are similar to the coatings found on top of the 'clean' sand grains (Fig. 5), indicate the dominance of the clay coating removal mechanism in these samples.

The kinetic energy reached by coarse grains (C_1) during saltation is higher than for finer grains (i.e., sand in the N samples) (Kok et al., 2012), thereby enhancing their potential for aeolian abrasion. In addition, the relatively sharp-edged grains of C_1 have greater potential to break during saltation to produce coarse dust particles. Saltation of rounded sand like N_1 and N_2 was found to be less efficient than saltation of angular sand at generating dust in abrasion (Bullard et al., 2004; Kuenen, 1960; Whalley et al., 1982; Wright et al., 1998). In typical active desert sand dunes, where quartz sand grains (N_1, N_2) tend to be smaller and more rounded (compared to coastal sites like C_1), aeolian abrasion is therefore suggested to play a very minor role as a dust generator. In addition, the relatively large-sized quartz dust particles (20–63 μm) that may be released by abrasion will suspend for shorted distances in a wind event than fine dust (<20 μm) (Kok et al., 2017; Mahowald et al., 2014; Nenes et al., 2014). Consequently, dust emission by aeolian abrasion is likely to play a relatively small role in global dust emissions.

The dust emission flux (Table 1) recorded from all of our sand samples are considered as very low compared to those produced by many other global dust sources. For example, the results obtained for N_2 sample were 10 times lower than those received during aeolian wind tunnel experiments in natural (undisturbed) Loess soils (northern Negev – Israel), which contain more than 40% dust-sized particles under similar wind velocity of ~7 $m\,s^{-1}$ (Swet and Katra, 2016; Tanner et al., 2016). However, even the lower PM_{10} concentrations from active sands can be significant when considering the wide extent of dune fields around the globe (Crouvi et al., 2012). A quantitative assessment of the potential of dust emission from global active sand dunes is thus needed to establish its contribution to the global dust cycle.

It should be noted that the aeolian saltation and dust emission in our experiments differ from natural settings in two key ways. First, whereas our experiments sustained a constant wind velocity and direction over a long duration to utilize the full emission potential of the sand bed, typical wind gust events that enable dust emission are significantly shorter in time. Second, whereas dust was only emitted from the wind tunnel during any particular experimental run, surface dust supply in natural sand dunes can be renewed by deposition of dust originating from nearby source areas. Thus, the depletion of dust under sustained wind and non-renewing conditions may have led to lower dust emission rates in our experiments than in similar natural settings. However, at this study we were looking at the relative contributions of different dust emission mechanisms rather than trying to derive an absolute dust emission law.

5. Conclusions

Large discrepancies in global dust emission models arise from a number of major gaps in our understanding of the dust emission mechanisms from different source areas. This study utilized aeolian experiments to explore the potential for dust emission from sands containing different sample compositions, and to distinguish the different mechanisms of dust generation from sand. We provided empirical evidence that dust can be emitted from active sands under natural conditions of saltation, were significantly higher PM_{10} concentrations were generated from sands that initially contained more than 2% dust.

The results obtained in this study provide insight into the dust generation mechanisms from active sand dunes. Our results indicate that the dominant dust emission mechanism over time for typical active sand dunes (<2% dust content) is clay coatings removal, with a relatively small contribution from re-emission of loose-settled dust. In sands containing higher amounts of dust-sized particles, the relative contribution of the re-emission mechanism increases drastically.

Despite the commonly accepted hypothesis for dust emission from active sands by the aeolian abrasion mechanism, this study suggests, based on analyses of emitted dust particles, that abrasion has only a minor contribution to dust generation from active sands, and largely produces coarse dust particles (>30 μm). Although the dust emission rates from sand recorded in this study are lower in comparison to emission rates from classic dust sources of non-sandy soils, the spatial extent of sand bodies is substantial, such that they should be taken into consideration in determining global dust emissions. Further analyses of the characteristics of dust emitted from sand dunes, such as chemical composition and size distribution, are needed for better representation of dust in climate models.

Acknowledgements

We thank Yue Huang for her help in sand sampling in Oceano dunes and for providing comments that helped improve the manuscript. We also thank the two anonymous reviewers for their useful comments on the manuscript. The study was supported by a grant from the United States–Israel Binational Science Foundation (2014178), and by the U.S. National Science Foundation (NSF) Postdoctoral Fellowship EAR-1249918 to R.L.M. and NSF grant AGS-1358621 to J.F.K.

Appendix A. Supplementary material

Supplementary material related to this article can be found online at https://doi.org/10.1016/j.epsl.2018.11.013.

References

Ahlbrandt, T.S., 1979. Textural parameters of aeolian deposits. In: McKee, E.D. (Ed.), A Study of Global Sand Seas. In: U. S. Geol. Surv. Prof. Pap., vol. 1052, pp. 21–52.

Alfaro, S.C., Gaudichet, A., Gomes, L., Maillé, M., 1997. Modeling the size distribution of a soil aerosol produced by sandblasting. J. Geophys. Res., Atmos. 102 (D10), 11239–11249. https://doi.org/10.1029/97JD00403.

Ashkenazy, Y., Yizhaq, H., Tsoar, H., 2012. Sand dune mobility under climate change in the Kalahari and Australian deserts. Clim. Change 112 (3–4), 901–923. https://doi.org/10.1007/s10584-011-0264-9.

Bagnold, R.A., 1937. The transport of sand by wind. Geogr. J. 89 (5), 409. https://doi.org/10.2307/1786411.

Bedrossian, T.L., Schlosser, J.P., 2007. Review of Vegetation Islands, Executive Summary, Oceano Dunes SVRA. California Geological Survey, Sacramento, CA.

Bhattachan, A., D'Odorico, P., Baddock, M.C., Zobeck, T.M., Okin, G.S., Cassar, N., 2012. The Southern Kalahari: a potential new dust source in the Southern Hemisphere? Environ. Res. Lett. 7 (2), 24001. https://doi.org/10.1088/1748-9326/7/2/024001.

Bullard, J.E., White, K., 2005. Dust production and the release of iron oxides resulting from the aeolian abrasion of natural dune sands. Earth Surf. Process. Landf. 30 (1), 95–106. https://doi.org/10.1002/esp.1148.

Bullard, J.E., McTainsh, G.H., Pudmenzky, C., 2004. Aeolian abrasion and modes of fine particle production from natural red dune sands: an experimental study. Sedimentology 51 (5), 1103–1125. https://doi.org/10.1111/j.1365-3091.2004.00662.x.

Bullard, J.E., McTainsh, G.H., Pudmenzky, C., 2007. Factors affecting the nature and rate of dust production from natural dune sands. Sedimentology 54 (1), 169–182. https://doi.org/10.1111/j.1365-3091.2006.00827.x.

Charnay, B., Barth, E., Rafkin, S., Narteau, C., Lebonnois, S., Rodriguez, S., Du Pont, S.C., Lucas, A., 2015. Methane storms as a driver of Titan's dune orientation. Nat. Geosci. 8 (5), 362. https://doi.org/10.1038/ngeo2406.

Claudin, P., Andreotti, B., 2006. A scaling law for aeolian dunes on Mars, Venus, Earth, and for subaqueous ripples. Earth Planet. Sci. Lett. 252 (1–2), 30–44. https://doi.org/10.1016/j.epsl.2006.09.004.

Cooper, W.S., 1967. Coastal Dunes of California. Geological Society of America, pp. 1–147.

Crouvi, O., Amit, R., Enzel, Y., Porat, N., Sandler, A., 2008. Sand dunes as a major proximal dust source for late Pleistocene loess in the Negev Desert, Israel. Quat. Res. 70 (2), 275–282. https://doi.org/10.1016/J.YQRES.2008.04.011.

Crouvi, O., Schepanski, K., Amit, R., Gillespie, A.R., Enzel, Y., 2012. Multiple dust sources in the Sahara desert: the importance of sand dunes. Geophys. Res. Lett. 39 (13). https://doi.org/10.1029/2012GL052145.

Evan, A.T., Flamant, C., Fiedler, S., Doherty, O., 2014. An analysis of aeolian dust in climate models. Geophys. Res. Lett. 41 (16), 5996–6001. https://doi.org/10.1002/2014GL060545.

Evan, A.T., Fiedler, S., Zhao, C., Menut, L., Schepanski, K., Flamant, C., Doherty, O., 2015. Derivation of an observation-based map of North African dust emission. Aeolian Res. 16, 153–162. https://doi.org/10.1016/J.AEOLIA.2015.01.001.

Field, J.P., Belnap, J., Breshears, D.D., Neff, J.C., Okin, G.S., Whicker, J.J., Painter, T.H., Ravi, S., Reheis, M.C., Reynolds, R.L., 2010. The ecology of dust. Front. Ecol. Environ. 8 (8), 423–430. https://doi.org/10.1890/090050.

Huang, Y., Kok, J.F., Martin, R.L., Swet, N., Katra, I., Gill, T.E., Reynolds, R.L., Freire, L.S., 2018. Fine dust emissions from coastal Oceano Sand Dunes. J. Geophys. Res. https://doi.org/10.5194/acp-2018-692.

Huneeus, N., Schulz, M., Balkanski, Y., Griesfeller, J., Kinne, S., Prospero, J., et al., Zender, C., 2010. Global dust model intercomparison in AeroCom phase I. Atmos. Chem. Phys. Discuss. 10 (10), 23781–23864. https://doi.org/10.5194/acpd-10-23781-2010.

Jerolmack, D.J., Brzinski, T.A., 2010. Equivalence of abrupt grain-size transitions in alluvial rivers and eolian sand seas: a hypothesis. Geology 38 (8), 719–722. https://doi.org/10.1130/G30922.1.

Jerolmack, D.J., Reitz, M.D., Martin, R.L., 2011. Sorting out abrasion in a gypsum dune field. J. Geophys. Res. 116 (F2), F02003. https://doi.org/10.1029/2010JF001821.

Jickells, T.D., An, Z.S., Andersen, K.K., Baker, A.R., Bergametti, G., Brooks, N., et al., Torres, R., 2005. Global iron connections between desert dust, ocean biogeochemistry, and climate. Science (N.Y.) 308 (5718), 67–71. https://doi.org/10.1126/science.1105959.

Katra, I., Arotsker, L., Krasnov, H., Zaritsky, A., Kushmaro, A., Ben-Dov, E., 2014a. Richness and diversity in dust stormborne biomes at the southeast Mediterranean. Sci. Rep. 4, 5265. https://doi.org/10.1038/srep05265.

Katra, I., Yizhaq, H., Kok, J.F., 2014b. Mechanisms limiting the growth of aeolian megaripples. Geophys. Res. Lett. 41 (3), 858–865. https://doi.org/10.1002/2013GL058665.

Katra, I., Gross, A., Swet, N., Tanner, S., Krasnov, H., Angert, A., 2016a. Substantial dust loss of bioavailable phosphorus from agricultural soils. Sci. Rep. 6. https://doi.org/10.1038/srep24736.

Katra, I., Elperin, T., Fominykh, A., Krasovitov, B., Yizhaq, H., 2016b. Modeling of particulate matter transport in atmospheric boundary layer following dust emission from source areas. Aeolian Res. 20, 147–156. https://doi.org/10.1016/j.aeolia.2015.12.004.

Kok, J.F., Parteli, E.J.R., Michaels, T.I., Karam, D.B., 2012. The physics of wind-blown sand and dust. Rep. Prog. Phys. 75 (10), 106901. https://doi.org/10.1088/0034-4885/75/10/106901.

Kok, J.F., Mahowald, N.M., Fratini, G., Gillies, J.A., Ishizuka, M., Leys, J.F., Mikami, M., 2014a. An improved dust emission model – part 1: model description and comparison against measurements. Atmos. Chem. Phys. 14, 13023–13041. https://doi.org/10.5194/acp-14-13023-2014.

Kok, J.F., Albani, S., Mahowald, N.M., Ward, D.S., 2014b. An improved dust emission model – part 2: evaluation in the Community Earth System Model, with implications for the use of dust source functions. Atmos. Chem. Phys. 14, 13043–13061. https://doi.org/10.5194/acp-14-13043-2014.

Kok, J.F., Ridley, D.A., Zhou, Q., Miller, R.L., Zhao, C., Heald, C.L., et al., Haustein, K., 2017. Smaller desert dust cooling effect estimated from analysis of dust size and abundance. Nat. Geosci. 10 (4), 274–278. https://doi.org/10.1038/ngeo2912.

Krasnov, H., Katra, I., Friger, M., 2016. Increase in dust storm related PM10 concentrations: a time series analysis of 2001–2015. Environ. Pollut. 213, 36–42. https://doi.org/10.1016/J.ENVPOL.2015.10.021.

Kuenen, P.H., 1960. Experimental abrasion 4: eolian action. J. Geol. 68 (4), 427–449. https://doi.org/10.1086/626675.

Mahowald, N., Albani, S., Kok, J.F., Engelstaeder, S., Scanza, R., Ward, D.S., Flanner, M.G., 2014. The size distribution of desert dust aerosols and its impact on the Earth system. Aeolian Res. 15, 53–71. https://doi.org/10.1016/J.AEOLIA.2013.09.002.

Marticorena, B., Bergametti, G., 1995. Modeling the atmospheric dust cycle: 1. Design of a soil-derived dust emission scheme. J. Geophys. Res., Atmos. 100 (D8), 16415–16430. https://doi.org/10.1029/95JD00690.

Martin, R.L., Kok, J.F., 2018. Distinct thresholds for the initiation and cessation of aeolian saltation from field measurements. J. Geophys. Res., Earth Surf. 123 (7), 1546–1565. https://doi.org/10.1029/2017JF004416.

Martin, R.L., Kok, J.F., Hugenholtz, C.H., Barchyn, T.E., Chamecki, M., Ellis, J.T., 2018. High-frequency measurements of aeolian saltation flux: field-based methodology and applications. Aeolian Res. 30, 97–114. https://doi.org/10.1016/j.aeolia.2017.12.003.

Muhs, D.R., Budahn, J.R., Johnson, D.L., Reheis, M., Beann, J., Skipp, G., et al., Jones, J.A., 2008. Geochemical evidence for airborne dust additions to soils in Channel Islands National Park, California. Geol. Soc. Am. Bull. 120 (1–2), 106–126. https://doi.org/10.1130/B26218.1.

Nenes, A., Murray, B., Bougiatioti, A., 2014. Mineral dust and its microphysical interactions with clouds. In: Mineral Dust. Springer Netherlands, Dordrecht, pp. 287–325.

Okin, G.S., Mahowald, N., Chadwick, O.A., Artaxo, P., 2004. Impact of desert dust on the biogeochemistry of phosphorus in terrestrial ecosystems. Glob. Biogeochem. Cycles 18 (2). https://doi.org/10.1029/2003GB002145.

Powers, M.C., 1953. A new roundness scale for sedimentary particles. J. Sediment. Petrol. 23 (117–119). https://doi.org/10.1306/D4269567-2B26-11D7-8648000102C1865D.

Pye, K., Tsoar, H., 2009. Aeolian Sand and Sand Dunes. Springer Berlin Heidelberg, Berlin, Heidelberg. https://doi.org/10.1007/978-3-540-85910-9.

Roskin, J., Katra, I., Blumberg, D.G., 2014. Particle-size fractionation of eolian sand along the Sinai–Negev erg of Egypt and Israel. Geol. Soc. Am. Bull. 126 (1–2), 47–65. https://doi.org/10.1130/B30811.1.

Runyon, K.D., Bridges, N.T., Ayoub, F., Newman, C.E., Quade, J.J., 2017. An integrated model for dune morphology and sand fluxes on Mars. Earth Planet. Sci. Lett. 457, 204–212. https://doi.org/10.1016/j.epsl.2016.09.054.

Schmerler, E., Katra, I., Kok, J.F., Tsoar, H., Yizhaq, H., 2016. Experimental and numerical study of Sharp's shadow zone hypothesis on sand ripple wavelength. Aeolian Res. 22, 37–46. https://doi.org/10.1016/J.AEOLIA.2016.05.006.

Shao, Y., 2008. Physics and Modelling Wind Erosion, vol. 37. Springer Science & Business Media.

Shao, Y., Raupach, M.R., Findlater, P.A., 1993. Effect of saltation bombardment on the entrainment of dust by wind. J. Geophys. Res. 98 (D7), 12719. https://doi.org/10.1029/93JD00396.

Shao, Y., Ishizuka, M., Mikami, M., Leys, J.F., 2011. Parameterization of size-resolved dust emission and validation with measurements. J. Geophys. Res. 116 (D8), D08203. https://doi.org/10.1029/2010JD014527.

Smalley, I.J., Vita-Finzi, C., 1968. The formation of fine particles in sandy deserts and the nature of 'desert' loess. J. Sediment. Res. 38 (3), 766–774. https://doi.org/10.1306/74D71A69-2B21-11D7-8648000102C1865D.

Sweeney, M.R., Lu, H., Cui, M., Mason, J.A., Feng, H., Xu, Z., 2016. Sand dunes as potential sources of dust in northern China. Sci. China Earth Sci. 59 (4), 760–769. https://doi.org/10.1007/s11430-015-5246-8.

Swet, N., Katra, I., 2016. Reduction in soil aggregation in response to dust emission processes. Geomorphology 268, 177–183. https://doi.org/10.1016/j.geomorph.2016.06.002.

Tanner, S., Katra, I., Haim, A., Zaady, E., 2016. Short-term soil loss by eolian erosion in response to different rain-fed agricultural practices. Soil Tillage Res. https://doi.org/10.1016/j.still.2015.08.008.

Tsoar, H., Blumberg, D.G., Wenkart, R., 2008. Formation and Geomorphology of the North-Western Negev Sand Dunes. Springer, Berlin, Heidelberg, pp. 25–48.

Vodonos, A., Friger, M., Katra, I., Krasnov, H., Zahger, D., Schwartz, J., Novack, V., 2015. Individual effect modifiers of dust exposure effect on cardiovascular morbidity. PLoS ONE 10 (9), e0137714. https://doi.org/10.1371/journal.pone.0137714.

Walden, J., White, K., 1997. Investigation of the controls on dune colour in the Namib Sand Sea using mineral magnetic analyses. Earth Planet. Sci. Lett. 125, 187–201. https://doi.org/10.1016/S0012-821X(97)00154-4.

Whalley, W.B., Marshall, J.R., Smith, B.J., 1982. Origin of desert loess from some experimental observations. Nature 300 (5891), 433–435. https://doi.org/10.1038/300433a0.

Wright, J., 2001. Making loess-sized quartz silt: data from laboratory simulations and implications for sediment transport pathways and the formation of "desert" loess deposits associated with the Sahara. Quat. Int. 76–77, 7–19. https://doi.org/10.1016/S1040-6182(00)00085-9.

Wright, J., Smith, B., Whalley, B., 1998. Mechanisms of loess-sized quartz silt production and their relative effectiveness: laboratory simulations. Geomorphology 23 (1), 15–34. https://doi.org/10.1016/S0169-555X(97)00084-6.

Yizhaq, H., Katra, I., 2015. Longevity of aeolian megaripples. Earth Planet. Sci. Lett. 422, 28–32. https://doi.org/10.1016/J.EPSL.2015.04.004.

Zaady, E., Katra, I., Yizhaq, H., Kinast, S., Ashkenazy, Y., 2014. Inferring the impact of rainfall gradient on biocrusts' developmental stage and thus on soil physical structures in sand dunes. Aeolian Res. 13, 81–89. https://doi.org/10.1016/J.AEOLIA.2014.04.002.

Zhang, J., Teng, Z., Huang, N., Guo, L., Shao, Y., 2016. Surface renewal as a significant mechanism for dust emission. Atmos. Chem. Phys. 16, 15517–15528. https://doi.org/10.5194/acp-16-15517-2016.